Single-Layer Dichroic Filters for Multifrequency Receivers at THz Frequencies

Daniel Montofre, Andrey Khudchenko, Fausto Patricio Mena, Ronald Hesper, and Andrey M. Baryshev

***Abstract*—In this work, we report the design, construction, and characterization of two free-standing single-layer frequency-selective surface structures to be used as dichroic filters in the THz range. Their spectral responses are aimed to fulfill a stringent band-pass performance in the atmospheric window between 600 and 725 GHz. Specifically, the dichroics have been required to allow a transmission of electromagnetic radiation of at least 90%, achieve a rejection in the stop-band lower than −25 dB, and have cross-polarization levels below −30 dB. All these specifications were demanded to be satisfied at normal and nonnormal beam incidence. We have studied dichroic filters with hexagonal patterns of two different apertures, a well-known single-hole geometry and, in order to enhance the spectral performance, a novel aperture geometry that we call the flower type. Their transmission characteristics were measured using a Fourier transform spectrometer. The electromagnetic simulations and experimental results not only show a good agreement but they demonstrate that the flower-type geometry can greatly outperform its single-hole counterpart achieving all the desired requirements. In this way, we demonstrate the feasibility of implementing single-layer systems at (sub)-THz frequencies suitable for low-noise astronomical applications.**

***Index Terms*—Astronomical applications, dichroic, frequency selective surface (FSS), millimeter/submillimeter wave, multifrequency receiver, single-layer, THz.**

I. Introduction

HISTORICALLY, electromagnetic waves in the THz range have remained one of the least exploited regions of the spectrum. This is basically because the technologies that deal with this type of waves are in a region between traditional microwave and optical technologies. Nevertheless, this situation is currently changing since an increasing commercial emphasis that has been placed on THz system in the last years [1], [2]. Moreover, the complementary use of THz instruments with heterodyne and Fourier transform techniques have allowed scientists from diverse fields (like astronomy, chemistry, or planetary and space exploration) to measure, catalog, and map thermal emission lines for a wide variety of light-weight molecules [3], [4]. The thermal emission lines from gases that appear in the Earth's stratosphere and upper troposphere (for instance, water, oxygen, chlorine, and nitrogen compound) have a particular importance. The spectral information of these components is vital to study the abundance, distribution, and reaction rates of elements involved in ozone destruction, global warming, and pollution monitoring [5]. Therefore, the development of new THz sensor technologies is very important to improve our understanding of the dynamics of our own Earth planet and, as well as, the atmospheric composition of new planets with conditions similar to Earth [6], [7].

Astronomy in the range of THz waves has also been highly boosted by the capabilities gained through the development of novel devices. Some examples are quantum-cascade lasers for LO generation, hot-electron bolometers for detection beyond 1.2 THz, and frequency-selective surface (FSS) for THz spectroscopy and filtering [8]. In addition, FSSs are widely used as dichroic filters, which allows either dividing a beam into two or combining beams from different sources into a single beam for further processing. The idea of dividing a beam is commonly found in astronomical applications since it has enabled the deployment of multiband receivers for radio astronomy, and multipixel system for current and future facilities on Earth, and stratospheric/space astronomy [9]–[12]. The benefits of a multireceiver systems are vast since they have allowed, so far, increasing the mapping speed and UV-plane coverage, enhance the phase calibration in high-frequency interferometric observations, and, moreover, they have the potential to provide unique information for future very long baseline interferometry (VLBI) observations [13], [14]. All these reasons, along with the continuous demand for an improved instrument sensitivity and signal quality, explain the increasing interest in THz instrumentation. Furthermore, such interest seems to continue increasing as new technologies are developed and production costs are reduced [15], [16].

In this work, we present the development and experimental demonstration of two free-standing single-layer dichroic filters aimed to be used in the THz range frequency. Since one of the of the motivations of this work is to enable true dual-band operation

Manuscript received June 1, 2020; revised August 26, 2020; accepted September 16, 2020. Date of publication September 21, 2020; date of current version November 3, 2020. The work of Daniel Montofré was supported by Conicyt through the Grant CONICYT-PCHA/DoctoradoNacional/2015-23190035. *(Corresponding author: Daniel Montofre.)*

Daniel Montofre is with the Group for Advanced Receiver Development, Chalmers University of Technology, 41296 Gothenburg, Sweden, and also with the Millimeter Wave Laboratory, Universidad de Chile, Santiago 1058, Chile (e-mail: danielmontofre@gmail.com).

Andrey Khudchenko is with the Astro Space Center, Lebedev Physical Institute of Russian Academy of Science, Moscow 117997, Russia (e-mail: A.Khudchenko@sron.nl).

Fausto Patricio Mena is with the Millimeter Wave Laboratory and the Department of Electrical Engineering, Universidad de Chile, Santiago 1058, Chile (e-mail: fpmena@u.uchile.cl).

Ronald Hesper and Andrey M. Baryshev are with the Kapteyn Astronomical Institute, University of Groningen, 9747, AD Groningen, The Netherlands (e-mail: r.hesper@astro.rug.nl; andrey@astro.rug.nl).

Color versions of one or more of the figures in this article are available online at https://ieeexplore.ieee.org.

Digital Object Identifier 10.1109/TTHZ.2020.3025692

TABLE I
DESIGN SPECIFICATIONS FOR A SUITABLE DICHROIC FILTER

Parameter	Frequency	Target Goal
Transmission	$600-725$ GHz	>90 %
Rejection	$211-275$ GHz	<-25 dB
Cross-polar	$211-725$ GHz	<-30 dB

in the Atacama large millimeter/submillimeter array (ALMA) telescope using existing receivers for Bands 9 (602–725 GHz) and 6 (211–275 GHz), we have concentrated in obtaining an excellent performance on those bands. The specific requirements are presented in Table I. Using a pattern with a novel aperture geometry, one of the studied filters allows to achieve all these stringent requirements outperforming other traditional geometries.

This article is structured as follows, in Section II we give a brief overview of the relevant theoretical considerations. In Section III, we describe the design process and show the simulated performance for each design. Section IV focuses on the fabrication processes used in each design. Finally, in Section V we present the Fourier transform spectrometer (FTS) setup and the experimental validation of the fabricated filters.

II. THEORETICAL BACKGROUND

Dichroic filters are a subgroup of FSSs, whose wide range of applications spans from the microwave to the near-infrared spectral region. In the most common implementation, a dichroic consists of a metallic plate which is periodically perforated. The simplest configuration for a dichroic is given by a single metal layer, perforated with circular apertures. Nevertheless, more complicated shapes have been used for improving different relevant aspects, such as transmittance stability, cross-polarization levels, increasing the bandwidth, or the resonance frequency with the incident angle. To this aim, many shaped apertures and multilayer configurations have been thoroughly studied [17]. For any dichroic the spectral response is determined by geometrical parameters, i.e., the shape and size of the apertures, the aperture spacing, and the thickness of metal layer. The most common aperture shapes are circular or rectangular, although cross-shaped apertures have also been widely used in [18], [19].

A general description for the spectral response of an electromagnetic wave going through a dichroic is presented in [20]. In this method, it is assumed that an incident plane wave striking upon the input face of a dichroic filter can be expanded into a set of Floquet modes [21]. These modes, in turn, must be matched to the waveguide modes inside the apertures (considering that each aperture behaves as a waveguide). At the output face of the waveguide, the dichroic filter acts as an array of apertures reradiating the incident electromagnetic wave, which is once again expanded into a set of Floquet modes. The spectral response of the dichroic filter is then obtained by matching the Floquet and waveguide modes.

Analytical expressions have been obtained for simple aperture shapes (like circles, squares, and crosses). For the case of circular apertures, each aperture is treated as a circular waveguide with a diameter d. Then, it is possible to define a band-pass, which occurs abovementioned the cutoff frequency and is given by [22]

$$\nu_c = 1.841\frac{c}{\pi d} \tag{1}$$

where c is the speed of light in free space. For frequencies below the cutoff frequency ν_c, the dichroic filter behaves as a plane mirror with a very low-loss rate. Furthermore, the aperture array of the dichoic filter also behaves as a two-dimensional grating. This behavior occurs for frequencies abovementioned the diffraction frequency ν_{diff}, which is given by [22]

$$\nu_{\text{diff}} = \frac{2c}{s\sqrt{3}} \tag{2}$$

where s is the aperture spacing. For frequencies higher than ν_{diff} electromagnetic waves fall into a region of increased insertion loss. This lossy region occurs when the wavelength of the incident wave is smaller than the aperture spacing s, thus part of the power is diffracted into the first diffraction lobe [23]. It is seen from (2) that a smaller aperture spacing results in a higher ν_{diff}, which establishes a clear caveat at the time of designing a dichroic filter for a specific purpose. There is an extra effect to be considered, which corresponds to the clear tradeoff between the thickness of the layer and the spectral response. Thin layers give a poor response, whereas thick layers exhibit a large ripple in the pass-band [24].

Additionally, the spectral response of a dichroic filter also depends on the angle of incidence of the incoming electromagnetic wave. It has been widely reported that when an incident angle is introduced ($\theta \neq 0^o$), the dichroic performance suffers a degradation proportional to that angle [24].

III. DESIGN OF THE PROPOSED MODELS

Designing a dichroic filter that accomplish all the design specifications listed in Table I represents a very challenging task. Given the high frequency at which this dichroic must operate, the electrical and mechanical constraints are quite strict. Special emphasis must be put on the subsequent construction process since we are dealing with geometrical parameters of the order of hundreds of microns.

In order to obtain the desired performance, we have studied two different geometries in hexagonal configuration, single holes (SH), and flower-type (FT), which are illustrated in Fig. 1. These geometries are defined by a common set of design parameters, layer thickness t, aperture spacing s, and hole diameter D. Moreover, the FT geometry has an additional parameter, the small-hole diameter d. The main motivations for studying this novel FT geometry were modifying the boundary conditions to improve the spectral properties, keeping the design easy (two circular perforations with different diameters), and make it compatible with the bee-hole pattern. The optimization of these geometries was made using HFSS [25]. We set as main optimization goal achieving a minimum of transmission of 90% in the pass-band ($600-725$ GHz). The secondary goals given to our script were keeping the rejection in the stop-band (211–275 GHz) below -25 dB to ensure a full reflection of the incoming wave, and maintaining cross-polar level below -30 dB to avoid leakage of power into high-order propagation

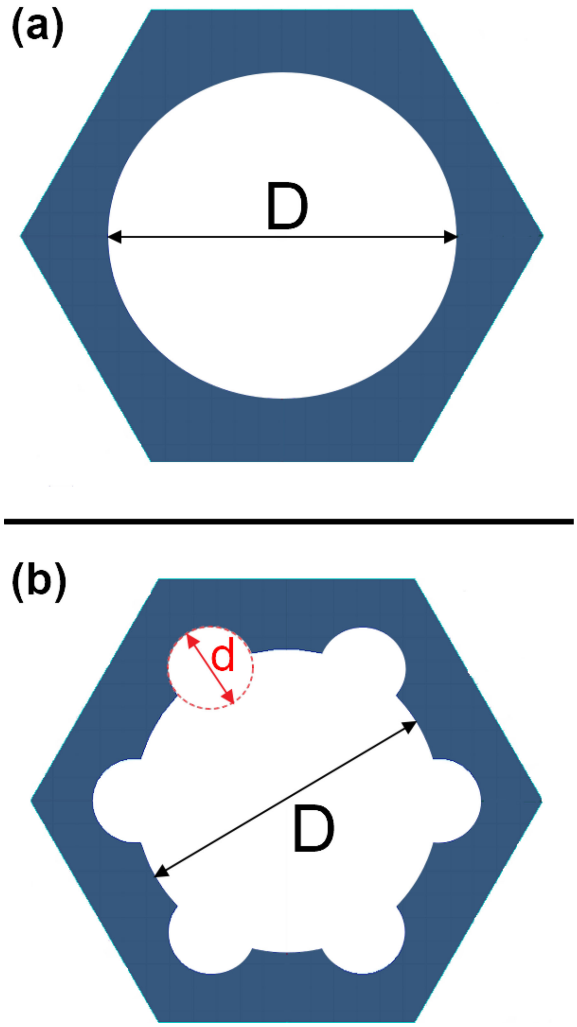

Fig. 1. Proposed dichroic filter configurations. In order to achieve the design specifications, we propose to optimize two different aperture shapes. (a) SH . (b) FT. The design parameters for each geometry are shown in Table II.

TABLE II
VALUES OF THE OPTIMIZATION PARAMETERS FOR EACH DICHROIC CONFIGURATION

	Single-hole	Flower-type
Parameter	μm	μm
layer thickness (t)	215	215
aperture spacing (s)	375	365
big hole diameter (D)	320	280
small hole diameter (d)	—	72

modes. These specifications were chosen in order to minimize the added noise temperature in each receiver band. On one hand, a dichroic with a transmission higher than 90% in the pass-band will introduce an extra noise of $\sim$33 K. On the other hand, a rejection lower than -25 dB in the stop-band assures than the noise added will be $\sim$1 K. These performance criteria were made considering that the dichroic will operate at room temperature conditions. The total noise added to each receiver band must be calculated in cascade, considering the dichroic as the first stage.

The set of parameters that optimize the performance are given in Table II. It was found, for both configurations, that a layer with

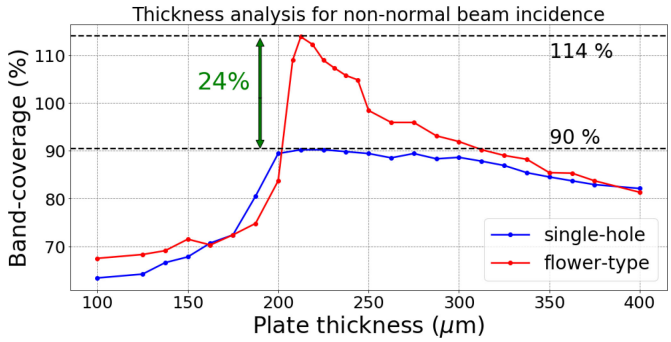

Fig. 2. Analysis of transmission as a function of the layer thickness for the two proposed configurations. Maximum band-coverage is obtained when $t = 215\,\mu m$ for both configurations. The FT configuration can reach a 24 % extra band-coverage, which represents a significant improvement.

a thickness of $\sim$215 μm gives the best performance, in terms of our main optimization goal (i.e., transmission), at nonnormal incidence. However, due to restrictions on the manufacturing processes available to us, the minimum thickness to implement the layers was $t = 275\,\mu$m. Thus, in order to estimate whether this difference of 60 μm is detrimental in the performance or not, we analyzed the dependence of the layer thickness on the transmittance. Since a degradation in performance is expected to be larger at nonnormal incidence, the analysis was restricted to only this case.

Fig. 2 shows the band-coverage as a function of the plate thickness t. In this context, the term band-coverage is used to indicate the fraction of the pass-band whose transmittance is over 90%. The maximum coverage is reached, in both configurations, for $t \approx 215$ μm. We see that the FT configuration can reach a band-coverage as high as 114% (i.e., covering more than is actually sought), whereas the SH only reaches a peak value of 90.2%. Hence, the FT can outperform the SH configuration by increasing the bandwidth in 24 %. Moreover, since the FT requires a thinner layer, this helps to make the fabrication more accurate and easier. All of these features put in evidence the significant improvement that FT provides when compared to the SH configuration. Since the thickness to be used in both configurations is $t = 275\,\mu$m, a band-coverage of around 89.4% and 91.1% are expected for SH and FT, respectively. We deem that the reached performance using the available layer is good enough for a prototype aimed to validate our results. In addition, Fig. 3 shows the band-coverage as a function of the angle of incidence (θ) for the chosen thickness. The plot shows that both configurations are equally sensitive to angular degradation.

Figs. 4 and 5 show the simulated performance at normal and nonnormal incidence ($\theta = 18^o$), respectively, for $t = 275\,\mu$m. A blue and green strips were included to indicate the stop-band and pass-band, respectively. Purple dashed lines in the plots show the design specifications, while cyan and yellow dashed lines indicate the cutoff (ν_c) and diffraction (ν_{diff}) frequency, respectively. Fig. 4 includes the simulated transmittance, rejection (equivalent to the transmittance in dB), and cross-polar loss. Fig. 5 only includes the simulated transmittance since the changes in the rejection and the cross polar are marginal with respect to the situation at normal incidence.

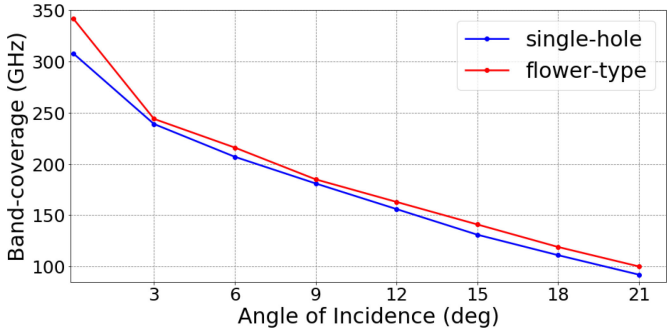

Fig. 3. Bandwidth as a function of the angle of incidence for the thickness to be used ($t = 275\ \mu$m). We see that the FT is less sensitive to angular degradation than the SH geometry. Angles of incidence $< 16^o$ can fully cover the target pass-band.

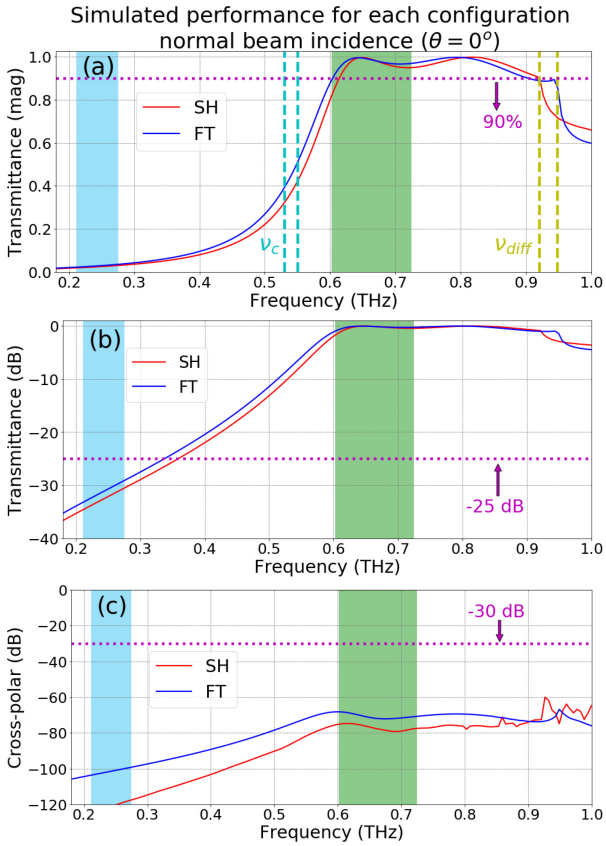

Fig. 4. Simulated. (a) Transmittance. (b) Rejection. (c) Cross-polar loss at normal incidence for the two proposed models with $t = 275\ \mu$m. The blue and green regions in the plot correspond to the pass-band (602–725 GHz) and the stop-band (211–275 GHz), respectively. Vertical dashed lines are included to indicate $\nu_c = 550$ GHz and $\nu_{\text{diff}} = 930$ GHz; horizontal dashed lines mark the design specifications.

Another important property of the studied dichroics can be drawn from Figs. 4 and 5. They show that the transmittance at normal incidence exhibits values over 90% until frequencies beyond 900 GHz for both configurations. However, this is different at nonnormal incidence since the angular dependence on the performance is evident. A notorious reduction of the band-coverage, and a small shift in the frequency cutoff toward lower frequencies are observed. Nevertheless, despite the reduction

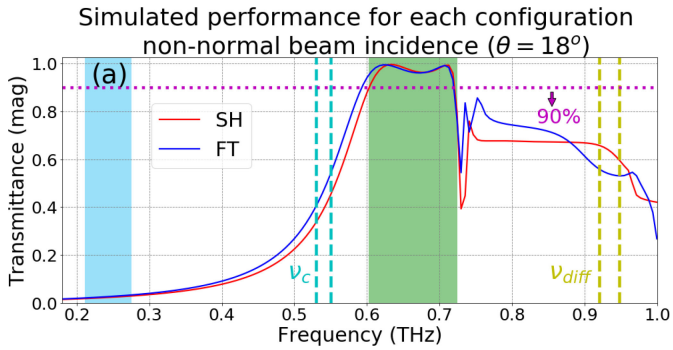

Fig. 5. Simulated transmittance at nonnormal incidence for the two proposed models with $t = 275\ \mu$m. The blue and green regions in the plot correspond to the pass-band (602–725 GHz) and the stop-band (211–275 GHz), respectively. Vertical dashed lines are included to indicate $\nu_c = 550$ GHz and $\nu_{\text{diff}} = 930$ GHz.

in the band-coverage, both configurations cover almost entirely the target frequency range with a transmittance over 90%. The simulated rejection in the Band 6 frequency range shows values in a range between -35 and -30 dB, therefore, satisfying the design specification. In the case of cross-polar performance, we see that the simulated value is around 40 dB, well below the specification.

In each proposed configuration ν_c and ν_{diff} were calculated using the parameters given in Table II. On one hand, at normal beam incidence, the theoretical values of ν_{diff} calculated by (2) are 922 and 948 GHz for SH and FT configuration, respectively. As shown in panel (a) of Fig. 4, these values show a very good agreement with the periodic boundary simulations. This agreement is missed at non-normal incidence (see Fig. 5) since tilting the dichroic changes the aperture appearance, and higher propagation modes are excited inside the waveguide. On the other hand, a good match between the analytical formulas and the periodic boundary simulations is seen for ν_c at normal and nonnormal incidence. The theoretical value obtained by (1) is 548 GHz for the SH configuration. The simulated transmittance of the FT configuration shows a similar behavior, but is down-shifted in $\sim$20 GHz. This feature makes reasonable to approximate the transmittance between the stop-band and pass-band of the FT configuration as a circular aperture of diameter 332 μm, and $\nu_c = 528$ GHz.

IV. Fabrication

Due to the clear difference in the aperture shape between both dichroics, two different methods were used to fabricate each proposed geometry. The SH dichroic was made out of brass and it was fabricated by drilling the holes with a computer numerical control (CNC) machine at the Physics Department of the University of Groningen, The Netherlands. The FT dichroic was made out of copper and it was fabricated by a commercial company using a combination of high-precision laser cutting and etching.

The fabricated dichroics are shown in Figs. 6 and 7. It is evident that none of the fabricated dichroics are free of manufacturing errors. In the case of the SH dichroic, the situation is

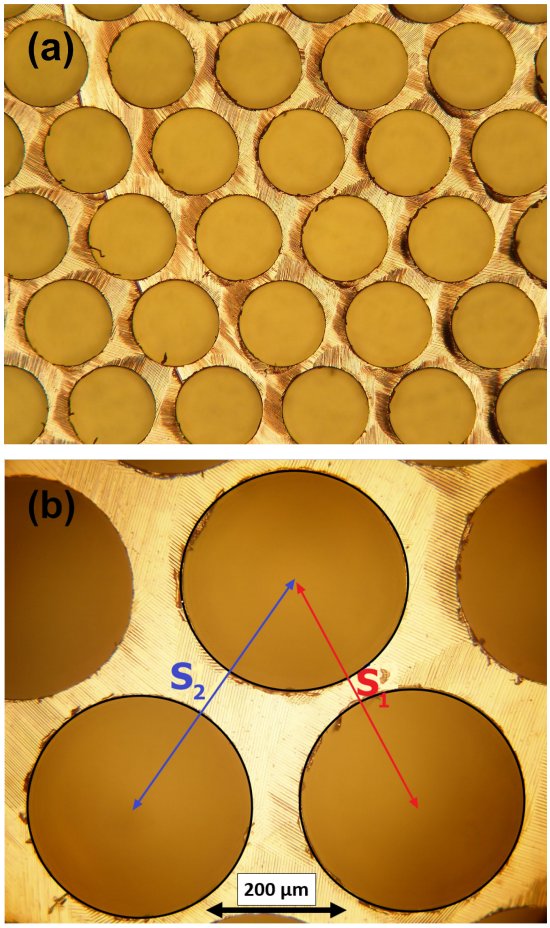

Fig. 6. (a) Fabricated SH dichroic made of brass. (b) Closeup showing an undesirable shift in spacing along one direction. A shifted spacing $s_2 = 415\mu$ m is observed (s_1 corresponds to the nominal value given in Table II). This imperfection breaks the hexagonal symmetry and it will produce changes in the performance. Moreover, imperfections in the surface are observed.

favorable but still not exempt from errors. The most notorious (and also the one that might produce an undesirable effect on the spectral properties) is the observed shift in the aperture spacing along one direction with a value $s_2 = 415\ \mu$m (s_1 corresponds to the nominal value given in Table II). The most likely explanation for this error is due to the selection of the path and accuracy that was given to the drilling tool. Additionally, some grooves are observed on the surface, which can increase the ohmic loss of this filter [26]. On the contrary, the FT dichroic seems to be the constructed with a higher accuracy. It is observed that the apertures and the spacing are quite homogeneous all over the surface on the front face. However, looking at the back face we see that part of the FT aperture shaped is missing and, instead, replaced with a circular aperture. Additionally, the plate of this dichroic presents an evident curvature, which is most likely result of thermal deformation when the laser was used to perforate the plate. A new simulation (not shown here) was made in order to include these errors and estimate their impact. An almost negligible difference of the spectral properties was observed in this new simulation. Therefore, we deem that these observed errors may not impact significantly the performance (which is actually demonstrated in the next section).

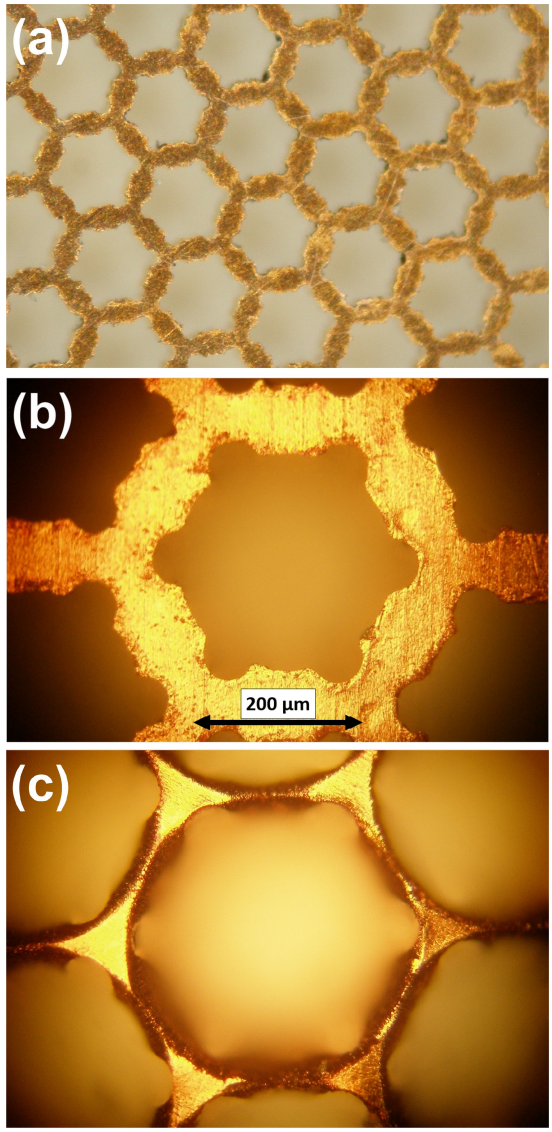

Fig. 7. (a) Fabricated FT dichroic made out of copper. (b) Closeup showing the front face reveals a high homogeneity in the aperture and spacing size. However, the "flower" shape of the aperture is missing on the back face. (c) Has been replaced with a circular aperture.

V. Experimental Validation

A. Measurement Setup

In order to measure the transmittance of the fabricated dichroics, we used a FTS, which consists of a Michelson interferometer, a wide band source based on a lamp, and a wide band detector (bolometer). The device-under-test (DUT) is put in a parallel beam between the FTS beam-splitter (BS) and the bolometer. In order to avoid spillover by the DUT the THz beam was reduced in size. For this, a diaphragm was placed between the BS and the DUT. A diagram of this THz interferometer is shown in Fig. 8. For each measurement we took a reference signal (S_{ref}) for further calibration. This signal was obtained by taking the DUT out of the setup, therefore, the interferograph obtained for this S_{ref} corresponds to the spectrum generated by the lamp. Then, we repeated the process, but this time including the

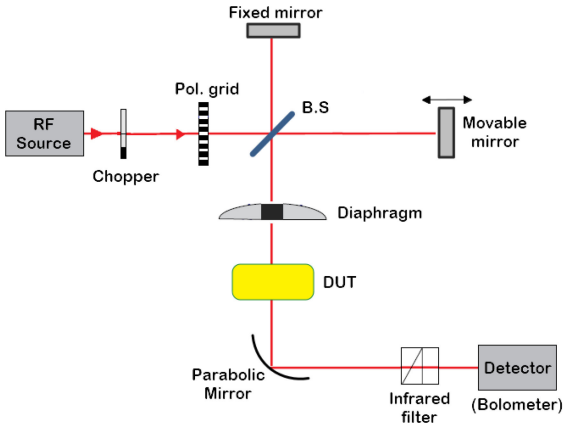

Fig. 8. Diagram of the FTS used to measure the transmission.

DUT. Thus, a second sampled spectrum was generated (S_{sampled}), which includes the contribution of the DUT. The transmittance (T) of the DUT was obtained by the ratio $S_{\text{sampled}}/S_{\text{ref}}$.

It was observed that the measurements at frequencies lower <350 GHz became very noisy. This noisy region appeared in all the measurements, but it is more noticeable in the inset (b) of Fig. 9. The reason why this happened is because the sensitivity of the used detector decreases as the frequency goes below 350 GHz and, it totally vanishes for frequencies lower than 200 GHz. Moreover, the dichroics present a rejection of <-20 dB for frequencies below 400 GHz. Thus, the ratio $S_{\text{sampled}}/S_{\text{ref}}$ for frequencies <350 GHz resulted in a signal dominated by noise. For this reason, the experimental data at frequencies lower than 300 GHz were removed from the plots in order to enhance their visualization.

B. *Characterization of the SH Dichroic*

The observed shift in the spacing (see Fig. 6) of the fabricated SH geometry has led to discrepancies between the measurements and the expected results shown in Figs. 4 and 5. From Fig. 9, we observe two clear consequences of breaking the symmetry of the aperture distribution, the band-pass is considerable lowered at both normal and nonnormal incidence and there is a decrease in the peak of transmittance. To explain this, new simulations were made. This time we implemented a bigger unit cell containing four apertures distributed asymmetrically as shown in the inset (d) of Fig. 9. In order to reduce the the size of the cell, and therefore, the computation time, a rhomboidal unit cell was used (instead of a hexagonal cell). The position of each aperture was shifted a certain distance with the intention of reproducing the observed aperture distribution shown in Fig. 6. In addition, we also included in the simulations the imperfections of the surface. This was made by reducing the bulk conductivity of the material to 20% of the value given in the HFSS material library [25].

The panels (a) and (b) of Fig. 9 compare the results of the new simulations with the experimental data. The blue line corresponds to a lossless asymmetric aperture distribution, while red line correspond to a lossy asymmetric distribution. We see that the former makes a fair match with the experiments but

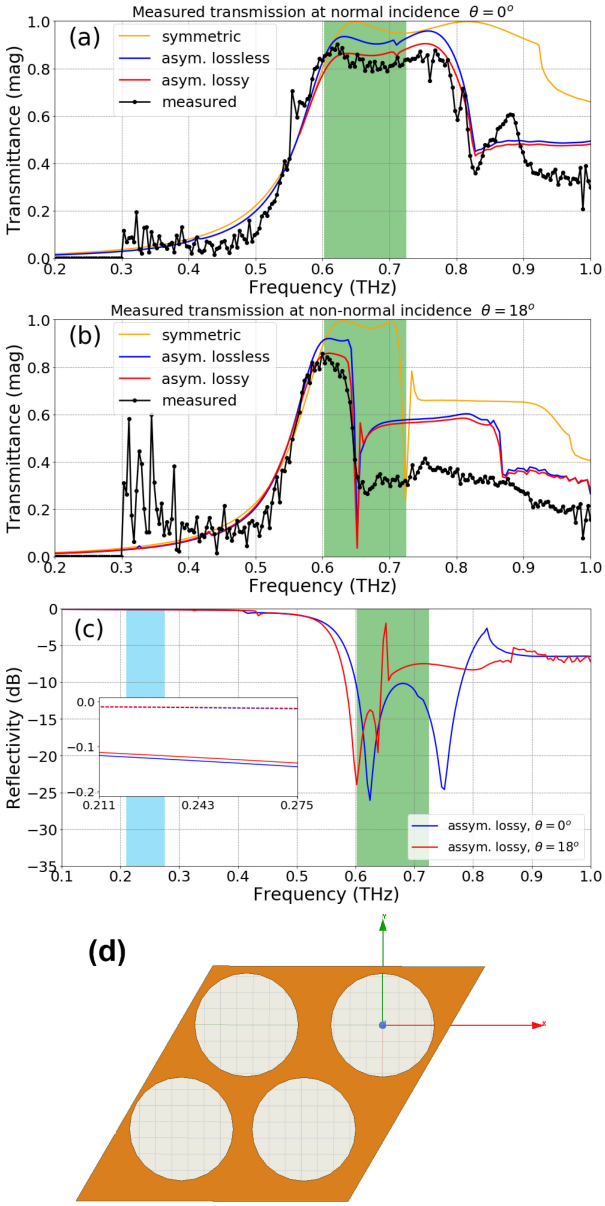

Fig. 9. Measurements versus simulation for SH filter. (a) Normal incidence. (b) Nonnormal incidence. (c) Simulations of reflectivity were also made in order to evaluate the impact in the stop-band. (d) Cell with an asymmetric aperture distribution, according to the fabricated dichroic, was also simulated. A better agreement is obtained when this cell and ohmic losses were included in the simulations.

a discrepancy in the peak value of transmittance is observed. Including a finite conductivity makes a better match with the experimental data. The transmittance shown in Figs. 4 and 5 were included with a yellow line for comparison. The measurements reveal that at normal incidence the transmittance reaches a maximum of $\sim 87\%$, whereas at nonnormal incidence the peak of value barely reaches $\sim 80\%$. This decrease in transmittance results as a consequence of the angular degradation that occurs at nonnormal incidence and, it is increased by the fabricated defects presented in it. In addition, the surface roughness has also a significant impact on the reflected low frequency band. The panel (c) of Fig. 9 shows the simulated reflectivity of the

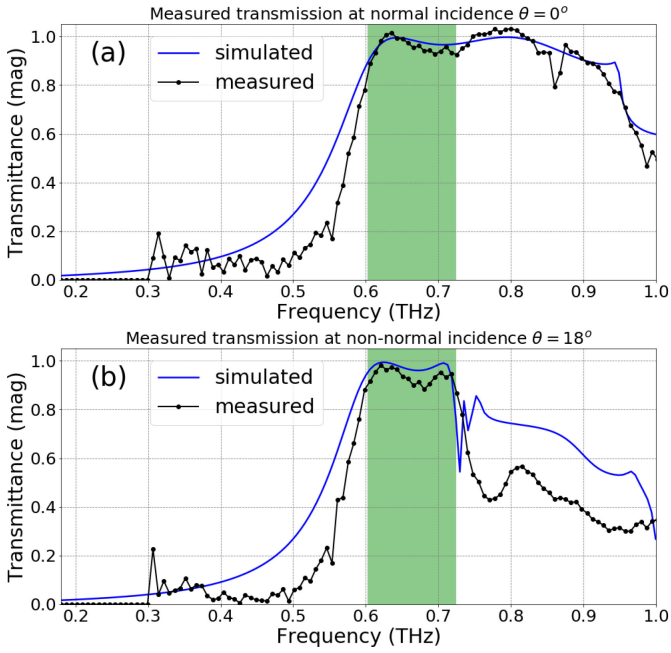

Fig. 10. Measurements versus simulation for FT filter. (a) Normal incidence (b) Nonnormal incidence. A good agreement is observed in both cases.

asymmetric apertures distribution. The inset shows a closeup of the stop-band region. Solid and dashed lines correspond to the lossy and lossless case, respectively. This result put in evidence that a degradation in reflectivity is mainly produced by the surface roughness, and it can reduce the reflectivity efficiency up to 97%, therefore, increasing the noise insertion up to $\sim$9.3 K.

C. Characterization of the FT Dichroic

Fig. 10 shows the comparison between measurements and simulations at normal and nonnormal incidence of the FT dichroic. First, an excellent agreement is observed at normal incidence. The measurements exhibit a sharper cutoff and, the frequency point where the cutoff occurs is slightly up-shifted. Second, the results at nonnormal incidence are also in good agreement. A similar feature for the cutoff frequency is observed, and, additionally, there is an small decrease in the level of transmittance. Despite this drop-off, the transmittance reaches a peak value $\sim$97% at 622 GHz, and a minimum of $\sim$87% within the pass-band. We believe that the cutoff shift occurs due to small defects of fabrication, specifically, the slightly conical shape of the apertures at the back face. As reported in [27], the measured cutoff frequency of fabricated dichroic filters is usually sensitive to the fabrication tolerances, while other filter properties remain similar. The discrepancy in transmittance can be also consequence of the conical shape at the back face. Since, as reported in [28], an increased loss of the propagation modes inside a circular waveguide occurs when the radius varies along the transverse direction. This loss is more evident at nonnormal incidence since it depends on the relative phase of the propagation modes.

Despite of the small difference in transmittance at nonnormal beam incidence, the experimental results demonstrate the advantage in performance of this novel geometry. This is particularly remarkable considering that the presented filter is a single-layer system operating at THz frequencies and with a bandwidth of $\sim$120 GHz.

VI. Conclusion

We have proposed two configurations for a dichroic filter that present a high transmission in the atmospheric window between 602–725 GHz. One novel aperture shape was presented (the socalled "FT" geometry), which has the potential to increase the transmitted frequency range by 24% at nonnormal beam incidence when the optimal layer thickness is chosen. Given the high operation frequency at which these dichroics were designed, small errors in the fabrication can lead to a break in the periodicity of the array, and thus, worsen the expected performance. This observation emphasizes the importance of tolerances during fabrication. The work presented here demonstrates that dichroics based on single layer system represent a good and competitive option for low-noise THz astronomical applications. The advantage of single-layer system over more complicated layer configuration is clear at the time of looking alternatives with lower cost and high repeatability. However, in order to obtain reliable results, high accuracy fabrication method, like laser cutting, must be used. The authors also believe that as new fabrication technologies arise, this works opens the possibility of looking for new aperture geometries suitable for high-performance dichroic filters.

Acknowledgment

The authors would like to thank J. Adema from the NOVA Sub-mm Instrumentation Group for all the logistic involved in the manufacturing process.

References

[1] P. H. Siegel, "Terahertz technology," *IEEE Trans. Microw. Theory Techn.*, vol. 50, no. 3, pp. 910–928, Mar. 2002.
[2] D. S. Wang, B. J. Chen, and C. H. Chan, "High-selectivity bandpass frequency-selective surface in Terahertz band," *IEEE Trans. Terahertz Sci. Technol.*, vol. 6, no. 2, pp. 284–291, Mar. 2016.
[3] P. H. Siegel, "Thz instruments for space," *IEEE Trans. Antennas Propag.*, vol. 55, no. 11, pp. 2957–2965, Nov. 2007.
[4] W. Wild, "Terahertz heterodyne technology for astronomy and planetary science," in *Proc. Joint 32nd Int. Conf. Infrared Millimeter Waves 15th Int. Conf. Terahertz Electron.*, Sep. 2007, pp. 323–325.
[5] P. G. Steffes and B. M. Karpowicz, "Microwave remote sensing of planetary atmospheres: From Staelin and Barrett to the NASA Juno Mission," in *Proc. IEEE Int. Geosci. Remote Sens. Symp.*, Jul. 2008, vol. 1, pp. I–130–I–133.
[6] R. Dickie, R. Cahill, V. Fusco, H. S. Gamble, and N. Mitchell, "Thz frequency selective surface filters for earth observation remote sensing instruments," *IEEE Trans. Terahertz Sci. Technol.*, vol. 1, no. 2, pp. 450–461, Nov. 2011.
[7] T. Hagelschuer *et al.*, "A compact 4.75-THz source based on a quantum-cascade laser with a back-facet mirror," *IEEE Trans. Terahertz Sci. Technol.*, vol. 9, no. 6, pp. 606–612, Nov. 2019.
[8] S. S. Dhillon *et al.*, "The 2017 terahertz science and technology roadmap," *J. Phys. D, Appl. Phys.*, vol. 50, no. 4, Jan. 2017, Art. no. 043001.
[9] N. Hurtado *et al.*, "Optics and cryogenics for the 1.1 THz multi-pixel heterodyne receiver for APEX," *Proc. SPIE*, vol. 9153, pp. 716–729, 2014.

[10] Carter M *et al.*, "The emir multi-band mm-wave receiver for the IRAM 30-m telescope," *Astronomy Astrophy.*, vol. 538, 2012, Art. no. A89.
[11] D. Farrah *et al.*, "Review: Far-infrared instrumentation and technological development for the next decade," *J. Astronomical Telescopes, Instrum., Syst.*, vol. 5, Apr. 2019, Art. no. 020901.
[12] M. C. Wiedner *et al.*, "A proposed heterodyne receiver for the origins space telescope," *IEEE Trans. Terahertz Sci. Technol.*, vol. 8, no. 6, pp. 558–571, Nov. 2018.
[13] M. J. Rioja, R. Dodson, T. Jung, and B. W. Sohn, "The power of simultaneous multifrequency observations for mm-VLBI: Astrometry up to 130 GHz with the kvn," *Astronomical J.*, vol. 150, no. 6, Dec. 2015, Art. no. 202.
[14] T. R. Hunter *et al.*, "Dual frequency 230/690 GHz interferometry at the submillimeter array," to be published.
[15] S. S. Dhillon *et al.*, "The 2017 terahertz science and technology roadmap," *J. Phys. D, Applied Phys.*, vol. 50, no. 4, Jan. 2017, Art. no. 043001.
[16] D. M. Mittleman, "Perspective: Terahertz science and technology," *J. Appl. Phys.*, vol. 122, no. 23, 2017, Art. no. 230901.
[17] S. Biber, M. Bozzi, O. Gunther, L. Perregrini, and L. Schmidt, "Design and testing of frequency-selective surfaces on silicon substrates for submillimeter-wave applications," *IEEE Trans. Antennas Propag.*, vol. 54, no. 9, pp. 2638–2645, Sep. 2006.
[18] T. Manabe, K. Kikuchi, S. Ochiai, and T. Nishibori, "Dual-polarization jerusalem-cross slot type FSS for a submillimeter-wave band," in *Proc. Int. Symp. Antennas Propag.*, Nov. 2015, pp. 1–3.
[19] C. Winnewisser, F. T. Lewen, M. Schall, M. Walther, and H. Helm, "Characterization and application of dichroic filters in the 0.1-3-THz region," *IEEE Trans. Microw. Theory Techn.*, vol. 48, no. 4, pp. 744–749, Apr. 2000.
[20] C.-C. Chen, "Transmission of microwave through perforated flat plates of finite thickness," *IEEE Trans. Microw. Theory Techn.*, vol. MTT-21, no. 1, pp. 1–6, Jan. 1973.
[21] R. Collin, I. Antennas, and P. Society, *Field Theory of Guided Waves*, (Series IEEE/OUP Series on Electromagnetic Wave Theory). Piscataway, NJ, USA: IEEE Press, 1990.
[22] D. H. Kim, W. Mohyuddin, D. S. Woo, H. C. Choi, and K. W. Kim, "Design of a 75-140 GHz high-pass printed circuit board dichroic filter," *Rev. Sci. Instrum.*, vol. 88, no. 3, 2017, Art. no. 034704.
[23] A. Hessel and A. A. Oliner, "A new theory of wood's anomalies on optical gratings," *Appl. Opt.*, vol. 4, no. 10, pp. 1275–1297, Oct. 1965.
[24] P. A. R. Ade, G. Pisano, C. Tucker, and S. Weaver, *"A review of metal mesh filters*," *Proc. SPIE,* vol. 6275, 2006, Art. no. 62750U.
[25] HFSS Ansoft, ver. 19.1.0, Ansoft Corp., Pittsburgh, PA, USA, 2018. [Online]. Available: https://www.ansys.com/products/electronics/ansys-hfss.
[26] S. P. Morgan, "Effect of surface roughness on eddy current losses at microwave frequencies," *J. Appl. Phys.*, vol. 20, no. 4, pp. 352–362, 1949.
[27] M. Bozzi, "Electromagnetic modeling of quasi-optical filters and frequency multipliers," Ph.D. dissertation, Dept. Electron., Universitá Degli Studi DI Pavia, Pavia, Italy, 2000.
[28] J. Shafii and R. J. Vernon, "Investigation of mode coupling due to ohmic wall losses in overmoded uniform and varying-radius circular waveguides by the method of cross sections," *IEEE Trans. Microw. Theory Techn.*, vol. 50, no. 5, pp. 1361–1369, May 2002.

Daniel Montofré received the double Ph.D. degree in electrical engineering from the Universidad de Chile, Santiago, Chile, and the University of Groningen, Groningen, The Netherlands, in 2020.

He is a Postdoctoral Researcher with the Group for Advanced Receiver Development, Gothenburg, Sweden. His research interests focused on the development of new instruments for millimeter/submillimeter astronomical applications with special interest in multifrequency receivers for VLBI, and passive devices for THz heterodyne detection.

Andrey Khudchenko received the M.S. degree in applied physics and mathematics and the Ph.D. degree in radio physics from the Moscow Institute of Physics and Technology, Moscow, Russia, in 2007 and 2009, respectively.

In 2009, he was a Researcher with the Kotel'nikov Institute of Radio Engineering and Electronics in Moscow. In 2009 to 2015, he was an Instrument Scientist with The Netherlands Institute for Space Research SRON and from 2015 to 2020, Instrument Scientist with the Kapteyn Astronomical Institute, University of Groningen. Since 2020, he joined Astro Space Center of Lebedev Physical Institute. The main activity is related to the development of new heterodyne THz instruments.

Fausto Patricio Mena received the B.S. degree in physics from the Escuela Politécnica Nacional, Quito, Ecuador, in 1994, and the M.Sc. and Ph.D. degrees in physics from the University of Groningen, Groningen, The Netherlands, in 2000 and 2004, respectively.

He is an Associate Scientist and Research Engineer with the Central Development Laboratory, National Radio Astronomy Observatory, Charlottesville, VA, USA, and an Adjunct Professor with the Electrical Engineering Department, Universidad de Chile, Santiago, Chile. In 2004, he joined the Netherlands Institute for Space Research (SRON), Groningen, The Netherlands, as an Instrument Scientist with the Low Energy Division. Between 2008 and 2020, he was an Assistant and Associate Professor with the Universidad de Chile where he cofounded the Radio Astronomical Instrumentation Group and the Millimeter Wave Laboratory. His research interests include the design, construction and testing of components and systems for millimeter and submillimeter wave instrumentation.

Ronald Hesper received the M.Sc. degree in experimental solid state physics from the University of Leiden, Leiden, The Netherlands, and the Ph.D. degree in experimental solid state physics from the University of Groningen, Groningen, The Netherlands.

Since 2000, he has been an Instrument Scientist with the Kapteyn Astronomical Institute, University of Groningen. From 2000 to 2008, he was involved in the technological development of the ALMA Band 9 receivers, including the process of industrialization, as well as related projects like the CHAMP+ mixer arrays for APEX; from 2008 to 2013, on the development of a sideband-separating mixer upgrade for the ALMA Band 9 receivers; and from 2013 to the beginning of 2015, on the industrialization of the ALMA Band 5 receivers. He is currently involved in the development of new (arrayable) heterodyne detector technologies at frequencies around 1 THz.

Andrey M. Baryshev received the master's degree (*summa cum laude*) in physical quantum electronics from the Moscow Institute of Physics and Technology, Moscow, Russia, in 1993, and the Ph.D. degree from the Technical University of Delft, Delft, The Netherlands, in 2005.

He is currently a Senior Instrument Scientist. Since 1998, he has been with the SRON Low Energy Astrophysics Division and the Kapteyn Astronomical Institute, University of Groningen, Groningen, The Netherlands. Since 2000, he has been involved in a joint effort to develop the SIS receiver (600–720 GHz) for ALMA. In 2013, he became an Associate Professor of astronomical instrumentation for the far-infrared with the Kapteyn Astronomical Institute, University of Groningen. His main research interests include the areas of heterodyne and direct detectors for large focal plane arrays at THz frequencies, and quasi-optical system design, and experimental verification.

Dr. Baryshev was the recipient of a Netherlands Organisation for Scientific earch-VENI grant for research on heterodyne focal plane array technology in 2008, and an EU commission Starting Researcher Grant for work on direct detector focal plane arrays in 2009.